Low temperature synthesis of $LiSi_2N_3$ nanobelts *via* molten salt nitridation and their photoluminescence properties

Feng Liang [a], Liang Tian [a], Haijun Zhang [a,*], Feng Liang [b], Simin Liu [b], Rongsheng Cheng [b], Shaowei Zhang [a,c,*]

a The State Key Laboratory of Refractories and Metallurgy, Wuhan University of Science and Technology, Wuhan 430081,China

b School of Chemical Engineering and Technology, Wuhan University of Science and Technology, Wuhan 430081,China

c College of Engineering, Mathematics and Physical Sciences, University of Exeter, Exeter Ex4 4QF, U.K.

Abstract

$LiSi_2N_3$ nanobelts were synthesized by using a novel low temperature molten salt nitridation technique using silicon and melamine as starting materials, and lithium chloride and sodium fluoride to form a reaction media. As-synthesized nanobelts were characterized by XRD, FESEM, HRTEM and SAED. The amount of $LiSi_2N_3$ increased with temperature. The optimal synthesis temperature for phase pure $LiSi_2N_3$ was at about 1200 °C, which was about 200 °C lower than that required by the conventional solid-state reaction routes. $LiSi_2N_3$ nanobelts about a few hundred long and 50-200nm in width were distributed uniformly in the final products. The possible growth mechanism was proposed based on the experimental results. Their photoluminescence emission at 459 nm (2.70 e*V*) at room temperature suggested that they could be potentially used in light-emitting nano-devices.

*Corresponding author. E-mail: zhanghaijun@wust.edu.cn (Prof. Haijun Zhang), s.zhang@exeter.ac.uk (Prof. Shaowei Zhang).

Keywords: Lithium-silicon-nitride; Nanobelts; Molten salt Nitridation; Photoluminescence.

1. Introduction

Replacement of traditional energy-wasting light sources such as incandescent lamps with energy-efficient LED lamps is considered as a major step towards reduction of electrical energy consumption worldwide.[1] In recent years, nitrides have received remarkable attention due to their nontoxicity, interesting luminescence properties, and potential applications as phosphors and pigments.[2,3]

Ternary lithium silicon nitrides are one of such interesting materials for luminescent applications.[4,5] Several ternary phases including $LiSi_2N_3$,[6] Li_2SiN_2,[7] Li_5SiN_3[8] and Li_8SiN_4[9] exist in the Li–Si–N ternary system, of which $LiSi_2N_3$ with a well-defined wurtzite type structure (space group $Cmc2_1$)[10] is of particular interest because of its high stability for practical applications. It is generally synthesized via the conventional solid-state reaction route using Li_3N and Si_3N_4 as the starting materials. Unfortunately, this synthesis method suffers from several disadvantages including requirements of high pressure and temperature,[6,11,12] and formation of heavily agglomerated $LiSi_2N_3$ with large particle size and spheroid morphology, which limits its functional applications[13]. To overcome these and to prepare high quality $LiSi_2N_3$ nanomaterials with novel morphologies and photoluminescence (PL) properties, an alternative processing route needs to be developed.

In response to this, $LiSi_2N_3$ nanobelts have been synthesized for the first time by using a novel low temperature molten salt nitridation (MSN) technique from relatively cheap Si powders and lithium chloride in this work. The effects of reaction temperature on phase composition and morphology of the final products were investigated, and PL properties of as-synthesized $LiSi_2N_3$ nanobelts examined.

2. Experimental procedure

Silicon (Si, purity ≥ 99 wt%, particle size ≤ 2 μm, Aladdin) and melamine ($C_3N_3(NH_2)_3$, purity ≥ 99 wt%, particle size ≤ 5 μm, Aladdin) powders were used as starting materials. They were pre-mixed and further combined with a LiCl-NaF binary salt containing 20 wt% NaF. The mixed powder batch was placed in an alumina crucible with a lid and heated at 5 °C/min in a N_2 protected alumina-tube furnace to a temperature between 900 and 1200 °C for 3h. After furnace-cooling to room temperature, the reacted mass was washed repeatedly with distilled water to remove the residual medium salt. The resultant powders were oven-dried overnight at 110 °C prior to further characterization.

Phases in product powders were identified by using an X-ray diffractometer (XRD, X'Pert Pro, Philips, Netherlands) with Cu-$K\alpha$ radiation (λ=1.5406 $\AA$) operated at 40 kV and 40 mA, with a scanning rate of 2° (2θ)/min and a step size of 0.02° (2θ). Morphologies of product phases were examined using a field emission scanning electron microscope (FESEM, Novo 400, FEI Co., USA), a transmission electron microscope (TEM, 2000F, Jeol Ltd., Japan) and selected area electron diffraction (SAED). UV-vis and room-temperature PL spectra were recorded respectively using a UV-vis spectrophotometer (Shimadzu UV-3600, Japan), and a fluorescence spectrophotometer (PerkinElmer LS 55, USA).

3. Results and discussion

Fig. 1 shows XRD patterns of product samples resultant from 3 h firing at various temperatures. At 900 °C, no $LiSi_2N_3$ was detected and only unreacted Si remained. At 1000 °C, $LiSi_2N_3$ started to appear and Si decreased, suggesting the formation reaction of $LiSi_2N_3$ just occur. On increasing the firing temperature to 1100 °C, $LiSi_2N_3$ peaks increased whereas those of Si decreased, implying more $LiSi_2N_3$ was formed at the expense of Si. On further increasing the temperature to 1200 °C, Si disappeared and only $LiSi_2N_3$ was identified, indicating the complete conversion from Si to $LiSi_2N_3$. This synthesis temperature was about 200 °C lower than that (1400 °C) required by the conventional solid-state reaction method,[4] indicating that the MSN technique introduced here can efficiently reduce the synthesis temperature of $LiSi_2N_3$. The composition of salt may play the key role in lowering the temperature, the reason was discussed in our previous literatures.[14,15,16]

Illustrated in Fig. 2 a-c are morphologies of samples resultant from 3 h firing at various temperatures in LiCl-NaF. At 1000 °C, many granular $LiSi_2N_3$ particles formed on the surface of Si (Fig. 2a). Upon increasing the temperature to 1100°C, large amounts of nanobelt-like $LiSi_2N_3$ phases appeared. On further increasing the temperature to 1200°C, $LiSi_2N_3$ nanobelts with a high aspect ratio of ~10 were formed (Fig. 2b,c). They were a few hundred nanometers in length and 50-200 nm in width, after epitaxial growth on the surface of Si (Fig. 2c).

The possible growth mechanism of these $LiSi_2N_3$ nanobelts can be schematically illustrated in the Fig. 2d and described as follows: in the initial stage, NaF in the LiCl-NaF binary salt diffused onto the Si surface and then reacted to form SiF_4(g) according to Reaction (1). On the other hand, melamine ($C_3N_3(NH_2)_3$) decomposed in-situ to produce NH_3 according to Reaction (2) (Step 1). In addition, LiCl interacted with Si(s), N_2(g) and NH_3(g), forming eutectic liquid droplets of Li-Si-N via Reaction (3) (Step 2). Upon oversaturation of the liquid droplets with $LiSi_2N_3$, the nucleation of $LiSi_2N_3$ would occur, followed by the growth of $LiSi_2N_3$ from the droplets (Step 3). With increasing the temperature to 1200 °C, more gaseous species (e.g. LiCl, SiF_4, and NH_3) were generated and dissolved in the droplets, sustaining the growth of $LiSi_2N_3$ via Reaction (4) (Step 4). Owing to the orthorhombic structure nature (i.e., cell parameters $a \neq b \neq c$), the different planes of $LiSi_2N_3$ possess different surface energy, and crystal surfaces with lower energies tend to serve as the enclosure surfaces. During the preparation process, the Li, Si and N elements preferred to deposit on the high energy surfaces, finally resulting in simultaneous formation of nanobelt structures. On the basis of the reaction mechanism mentioned above and the observation of $LiSi_2N_3$ small particles (Fig 2a), we proposed that the growth of the as-synthesized $LiSi_2N_3$ nanostructures was controlled by the classic VLS mechanism.[17]

$$4NaF(l)+Si(s) \rightarrow SiF_4(g)+4Na(g) \quad (1)$$

$$2C_3N_3\left(NH_2\right)_3(s) \rightarrow 3(CN)_2(g)+4NH_3(g)+N_2(g) \quad (2)$$

$$3LiCl(l)+6Si(s)+4N_2(g)+NH_3(g) \rightarrow 3LiSi_2N_3(s)+3HCl(g) \quad (3)$$

$$LiCl(g)+2SiF_4(g)+3NH_3(g) \rightarrow LiSi_2N_3(s)+8HF(g)+HCl(g) \quad (4)$$

TEM images were further performed along with the SAED patterns to assist identifying the crystalline structure of $LiSi_2N_3$ nanobelts resultant from 3 h firing at 1200 °C. Fig. 3a shows a low-magnification TEM image of a representative individual nanobelt, revealing that its aspect ratio was >10 and it had a smooth surface and a uniform width (about 150 nm). Fig. 3b further presents a high-resolution TEM (HRTEM) image of its edge area, showing that the interplaner distance was 0.33 nm which matched with the (111) plane of $LiSi_2N_3$. This result indicated that the $LiSi_2N_3$ nanobelt grew along the [111] direction, as suggested by the XRD results (Fig.1). Moreover, the SAED pattern (inset in Fig. 3b) confirmed that the $LiSi_2N_3$ nanobelt was single crystalline in nature.

The UV-vis absorption spectrum of as-synthesized $LiSi_2N_3$ nanobelts (Fig. 4a) shows nearly zero absorbance in the visible range but significant absorbance in the UV region. A narrow absorption peak centered at 221nm appeared, which corresponded to a band gap of ~5.61 e*V*. This value was smaller than that (at ~6.40 e*V*) reported previously for bulk $LiSi_2N_3$.[4] Such a shift in the present sample could be attributed to the saddle point transition in the band structure.[18] The optical band gap (OBG) estimated[19] from the UV-vis absorption spectrum of as-synthesized $LiSi_2N_3$ nanobelts was ~5.25 e*V* (see the inset in Fig. 4a). To further understand optoelectronic properties of as-synthesized $LiSi_2N_3$ nanobelts, their PL properties were also examined. Ultraviolet light used to excite the nanobelts was obtained from xenon lamp and its excitation wavelength was set at 221 nm. As seen from the room-temperature PL emission spectrum (Fig. 4b), intense luminescence in the violet-blue spectral range from 350 to 500 nm, with a main emission peak at around 459 nm (2.70 e*V*), occurred. Similar phenomena were also observed for BN nanoplates and AlN nanoneedles,[20,21] which are believed to arise from the surface effect (increased surface-to-volume ratios) and defect concentrations. Such explanation could also be used for present observed optical behavior of the as-synthesized $LiSi_2N_3$ nanobelts. However, detailed mechanisms on the PL properties of the $LiSi_2N_3$ nanobelts are not fully understood and require more systematic investigation. The intensive PL emission spectrum indicated that $LiSi_2N_3$ nanobelts prepared in this work could be potentially used in optical and optoelectronic devices such as LEDs, blue-light source, and UV detector.

4. Conclusions

A novel molten salt nitridation technique was successfully developed and used for the first time to synthesize single crystalline $LiSi_2N_3$ nanobelts. The synthesis temperature for phase pure $LiSi_2N_3$ was about 1200 °C, which was about 200 ^{o}C lower than that required by the conventional solid-state method. As-synthesized $LiSi_2N_3$ nanobelts were a few hundred nanometers long and 50-200 nm in width. The VLS growth mechanism is believed to have dominated the formation process of the $LiSi_2N_3$ nanobelts. The room-temperature PL spectrum suggested that as-synthesized $LiSi_2N_3$ nanobelts could be a promising candidate material for optical and optoelectronic applications.

Acknowledgement

This work was supported by the National Natural Science Foundation of China (51502216, 51472184, 51472185), Natural Science Foundation of Hubei Province (China, Contract No. 2013CFA086), Foreign cooperation projects in Science and Technology of Hubei Province (Contract No. 2013BHE002) and China Postdoctoral Science Foundation (2014M560631).

References

1. C. Che and R. S. Liu, *J. Phys. Chem. Lett.,* 2011, **2**, 1268-1277.
2. R. J. Xie, *J. Am. Ceram. Soc.,* 2013, **96**, 665-687.
3. P. Pust, V. Weiler, C. Hecht, A. Tücks, A. S. Wochnik, A. K. Henß, D. Wiechert, C. Scheu, P. J. Schmidt and W. Schnick, *Nat. Mater.,* 2014, **13**, 891-896.
4. Y. Q. Li, N. Hirosaki, R. J. Xie, T. Takeka and M. Mitomo, *J. Solid State Chem.,* 2009, **182**, 301-311.
5. Q. Wu, Y. Li, X. Wang, Z. Zhao, C. Wang, H. Li, A. Mao and Y. Wang, *RSC Adv.,* 2014, **4**, 39030-390306.
6. E. Narimatsu, Y. Yamamoto, T. Nishimura and N. Hirosaki, *J. Ceram. Soc. Jap.,* 2010, **118**, 837-841.
7. A. J. Anderson, R. G. Blair, S. M. Hick and R. B. Kaner, *J. Mater. Chem.,* 2006, **16**, 1318-1322.
8. A. T. Dadd and P. Hubberstey, *J. Chem. Soc.,* 1981, **77**, 1865-1870.
9. H. Yamane, S. Kikkawa and M. Koizumi, *Solid State Ion.,* 1987, **25**, 183-191.

10. M. Orth and W. Schnick, *Z. Anorg. Allg. Chem.,* 1999, **625**, 1426-1428.

11. J. Ding, Q. Wu, Y. Li, Q. Long, C. Wang and Y. Wang, *J. Am. Ceram. Soc.,* 2015, **98**, 2523-2527.

12. N. Tapia-Ruiz, M. Segalés and D. H. Gregory, *Coordin. Chem. Rev.,* 2013, **257**, 1978-2014.

13. X. G. Wan, J. M. Dong and D. Y. Xing, *Phys. Rev. B,* 1998, **58**, 6756.

14. J. Ye, S. Zhang and W. E. Lee, *J. Eur. Ceram. Soc.*, 2013, **33**, 2023-2029.

15. Z. Huang, H. Duan, J. Liu and H. Zhang, *Ceram. Int.*, 2016, **42**, 10482-10486.

16. Z. Huang, F. Li, C. Jiao, J. Liu, J. Huang, L. Lu, H. Zhang and S. Zhang, *Ceram. Int.*, 2016, **42**, 6221-6227.

17. Z. Peng, N Zhu, X. Fu, C. Wang, Z. Fu, L. Qi and H. Mao, *J. Am. Ceram. Soc.*, 2010, **93**, 2264-2267.

18. A. Zunger, A. Katzir and A. Halperin, *Phys. Rev. B,* 1976, **13**, 5560-5573.

19. Y. Stehle, H. M. Meyer, R. R. Unocic, M. Kidder, G. Polizos, P. G. Datskos, R. Jackson, S. N. Smirnov and I. V. Vlassiouk, *Chem. Mater.,* 2015, **27**, 8041-8047.

20. L. Ye, L. Zhao, F. Liang, X. He, W. Fang, H. Chen, S. Zhang and S. An, *Ceram. Int.*, 2015, **41**, 14941-14948.

21. S.H. Shah, G. Nabi, W.S. Khan, A. Majid, C. Cao, S. Ali, M. Hussain, A. Nabi, S. Ishaq and F. K. Butt, *Mater. Lett.,* 2013, **107**, 255-258.

Figure Captions:

Fig. 1 XRD patterns of product samples resultant from 3h firing at various temperatures.

Fig. 2 SEM images showing morphologies of product phases in samples resultant from 3 h firing in LiCl-NaF at various temperatures: (a) 1000 °C, (b) 1100 °C, (c) 1200 °C (inset shows a high-magnification image), and (d) schematic of the growth mechanism of $LiSi_2N_3$ nanobelts.

Fig. 3 TEM images of as-synthesized $LiSi_2N_3$ nanobelts. (a) A low-magnification TEM image of a representative individual nanobelt, (b) a high-resolution TEM image taken from the edge region of the nanobelt shown in (a) . The inset was the representative SAED pattern of the nanobelt.

Fig. 4 (a) UV-vis absorption spectrum and optical band gap analysis (inset), and (b) emission photoluminescence (PL) spectrum (λ_{ex}= 221 nm) of as-synthesized $LiSi_2N_3$ nanobelts.

Fig. 1

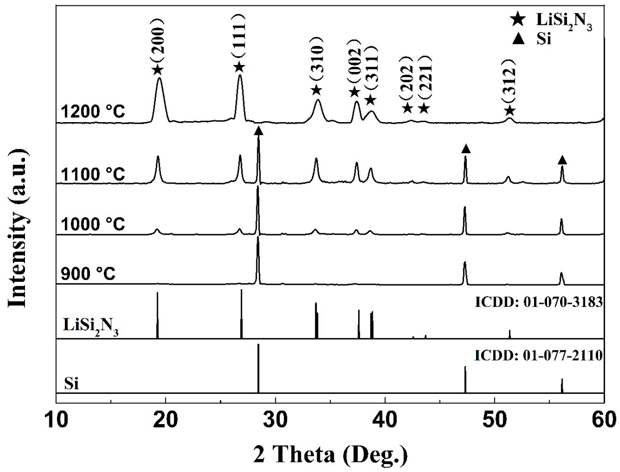
★ LiSi2N3
▲ Si
★(200)
★(111)
★(310)
★(002)
★(311)
★(202)
★(221)
★(312)
1200 °C
1100 °C
1000 °C
900 °C
ICDD: 01-070-3183
LiSi2N3
ICDD: 01-077-2110
Si
Intensity (a.u.)
10
20
30
40
50
60
2 Theta (Deg.)

Fig. 2

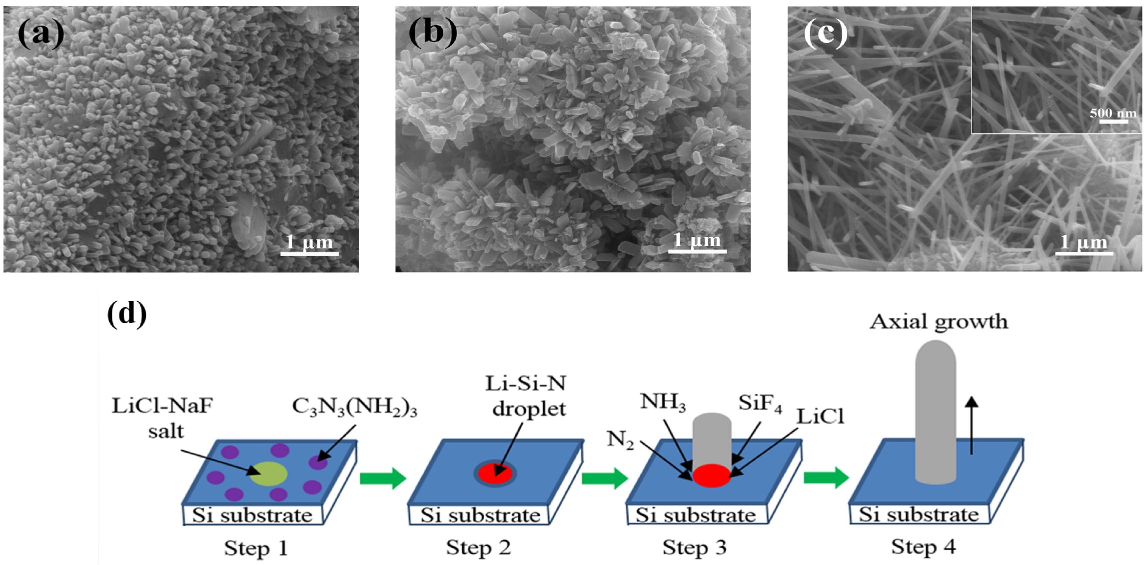
(a)
1 µm
(b)
1 µm
(c)
500 nm
1 µm
(d)
LiCl-NaF
salt
C3N3(NH2)3
Li-Si-N
droplet
NH3
SiF4
LiCl
N2
Axial growth
Si substrate
Step 1
Si substrate
Step 2
Si substrate
Step 3
Si substrate
Step 4

Fig. 3

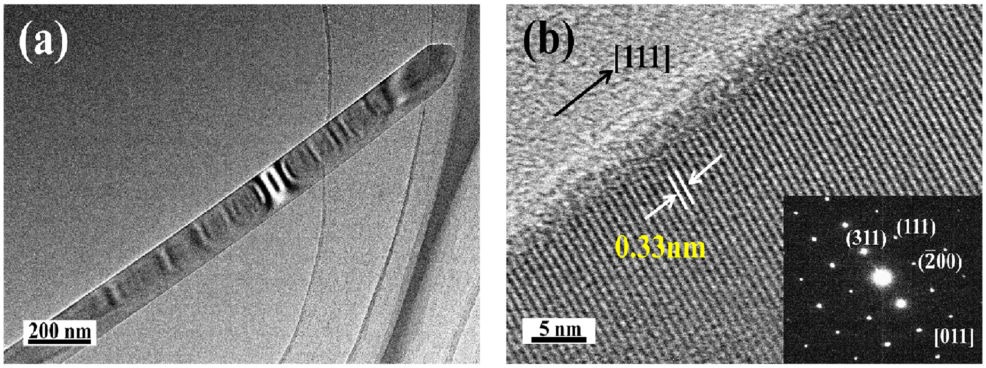

Fig. 4

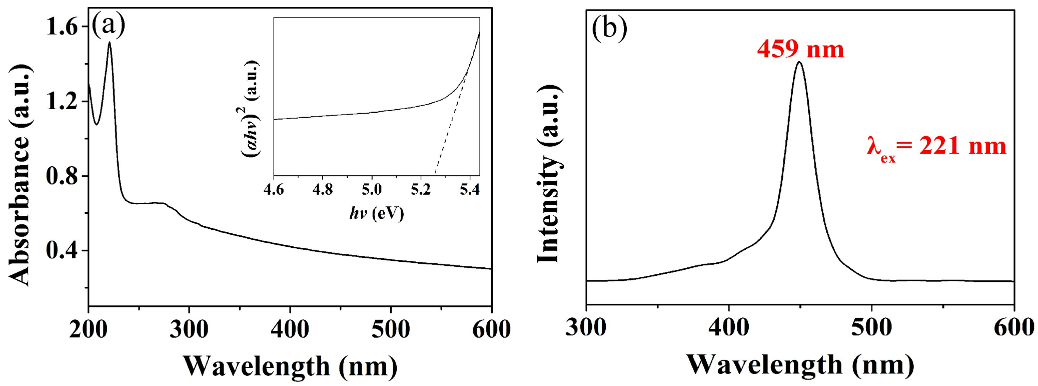
(a)
Absorbance (a.u.)
1.6
1.2
0.8
0.4
200
300
400
500
600
Wavelength (nm)
(αhν)^2 (a.u.)
4.6
4.8
5.0
5.2
5.4
hν (eV)
(b)
459 nm
λex= 221 nm
Intensity (a.u.)
300
400
500
600
Wavelength (nm)

Graphical Abstract

$LiSi_2N_3$ nanorods are synthesized using a novel low temperature MSN technique for the first time. The $LiSi_2N_3$ nanorods show an optical band gap of 5.25eV and exhibited an intense violet-blue PL emission from 350 nm to 500 nm with a main peak at around 459 nm in the room temperature.